Electric dipole sheets in BaTiO_{3}/BaZrO_{3} superlattices

Zhijun Jiang, Bin Xu, Fei Li, Dawei Wang, and C.-L. Jia

Phys. Rev. B **91**, 014105 — Published 14 January 2015

DOI: 10.1103/PhysRevB.91.014105

Electric dipole sheets in $BaTiO_3$/$BaZrO_3$ superlattices

Zhijun Jiang,[1] Bin Xu,[2] Fei Li,[1] Dawei Wang,[1,*] and C.-L. Jia[1,3]

[1]*Electronic Materials Research Laboratory–Key Laboratory of the Ministry of Education and International Center for Dielectric Research, Xi'an Jiaotong University, Xi'an 710049, China*

[2]*Physics Department and Institute for Nanoscience and Engineering, University of Arkansas, Fayetteville, Arkansas 72701, USA*

[3]*Peter Grünberg Institute and Ernst Ruska Centre for Microscopy and Spectroscopy with Electrons, Research Center Jülich, D-52425 Jülich, Germany*

Abstract

We investigate two-dimensional electric dipole sheets in the superlattice made of $BaTiO_3$ and $BaZrO_3$ using first-principles-based Monte-Carlo simulations and density functional calculations. Electric dipole domains and complex patterns are observed and complex dipole structures with various symmetries (e.g. $Pma2$, $Cmcm$ and $Pmc2_1$) are further confirmed by density functional calculations, which are found to be almost degenerate in energy with the ferroelectric ground state of the $Amm2$ symmetry, therefore strongly resembling magnetic sheets. More complex dipole patterns, including vortices and anti-vortices, are also observed, which may constitute the intermediate states that overcome the high energy barrier of different polarization orientations previously predicted by Lebedev [1]. We also show that such system possesses large electrostrictive effects that may be technologically important.

PACS numbers: 77.80.Dj, 77.80.Jk, 68.65.Cd, 77.65.Bn

I. INTRODUCTION

Two-dimensional (2D) magnetic systems have been an important topic in the study of magnetism[2–4]. The Ising model is such an important theoretical model that it had been investigated using analytical (e.g., mean-field theory) and numerical [e.g., Monte-Carlo (MC) simulations] methods[5–7]. More than just theoretical interest, certain real magnetic systems indeed have special magnetic structures, in particular the so-called magnetic sheets, i.e., layers containing magnetic moments separated by non-magnetic layers[8], examples including K_2NiF_4 and Sr_2RuO_4[9]. Such systems have interesting properties (e.g. nanoscale magnetic domains) and a common feature of them is that the energy difference between different structure and magnetic phases is very small[9–11]. On the other hand, it is interesting to note that similar structures comprised of *electric* dipoles are much less known. The concept of "arrays of nearly independent ferroelectrically ordered quasi-two-dimensional layers" was first clearly proposed by Lebedev in his investigation of $KNbO_3$/$KTaO_3$ superlattices (SLs)[12]. Here, via first-principles-based MC simulations, we will further point out the analogy between electric dipole sheets (quasi-two-dimensional ferroelectric layers) existing in the SL made of $BaTiO_3$ (BTO) and $BaZrO_3$ (BZO) to magnetic dipole sheets in terms of energy degeneracy and the complexity of dipole patterns.

The solid solution of BTO and BZO, which is chemically disordered and denoted by $Ba(Zr,Ti)O_3$ (BZT), is a well known ferroelectric material, most famous for its relaxor properties (see, e.g., Refs.[13–22] and references therein). Among its anomalous properties, the best known signature is perhaps the shift of the temperature T_m, where the susceptibility as a function of temperature peaks, with frequency used in the measurement of the susceptibility. Recently, Akbarzadeh *et al.*[17] developed a first-principles-based effective Hamiltonian to investigate disordered BZT. Based on this effective Hamiltonian, Sherrington[20] argued that BZT can be understood as soft spin-glass. Using the same effective Hamiltonian, MC simulations have shown that dipoles on Ti-containing sites are substantially larger than those on Zr-containing sites, which provides the possibility of having isolated electric dipoles in this type of materials. For instance, a SL made of alternating layers containing Ti and Zr ions will give rise to isolated planes of electric dipoles that resembles magnetic sheets.

However, it is unclear if such 2D electric dipole system indeed behaves like magnetic sheets in the sense that very complex dipole patterns exist. Note the recent study indicate large band of phonon frequencies along Γ-Z-R-X-Γ have similar large negative values, indicating various insta-

bilities, but only certain high-symmetry dipole patterns are computed via *ab initio* computations and compared to the ferroelectric ground state[1]. Moreover, on the application side, experiments have found that electrostriction effect is generally stronger in ordered systems than in disordered systems[23,24]. It is important to know if such effect also happens with lead-free BZT. As a matter of fact, disordered BZT contains Ti ion under various chemical environment, for instance, there could be 1, 2, ..., 6 Zr ions surrounding one Ti ion as its nearest neighbors. In addition, the distance from other Ti ions to a given Ti ion is also random. This randomness potentially harms physical properties of BZT that require the correlation of dipoles on many Ti ions. Ordered BZT offers certain level of freedom to address these two problems together because: (i) the distance between Ti ions are preconditioned; (ii) the chemical environment are uniform for every electric dipole in the 1:1 SL. In addition, confined dimensionality may also be an advantage to certain applications[25].

Therefore investigating chemically ordered BZT will expand our understanding of lead-free relaxors and may suggest systems that have better physical properties. Here we consider chemically ordered BZT SLs with alternating Ti and Zr layers grown along the $[001]$ direction. In such a structure, unlike the disordered BZT, large electric dipoles are restricted to each Ti-containing (001) planes[17], which significantly modifies the energy landscape of the system. As a consequence, novel phases are allowed and complex electric dipole patterns may form. In addition, the chemical environment of each large electric dipole is the same (since every Ti ion is surrounded by 4 Ti and 2 Zr ions as nearest neighbors), therefore giving rise to a single Debye-type relaxation mode in its dielectric responses, and distinguishing itself from disordered BZT. Moreover, comparing the electrostriction of ordered BZT to disordered BZT systems, we find that ordered BZTs indeed possess large electrostrictive coefficient, which may be exploited in applications. We also note such a structure is one of the ferroelectric-dielectric SLs, structurally similar to the $BaTiO_3$/ $SrTiO_3$, $PbTiO_3$/ $SrTiO_3$ and $Pb(Zr_{0.3},Ti_{0.7})O_3$/ $SrTiO_3$ SLs, which are actively investigated theoretically and experimentally[26–29].

II. METHOD

Practically, we simulate BZT SLs with alternating Ti and Zr layers along the $[001]$ direction [shown in the inset of Fig. 1(a)]. The first-principles-based effective Hamiltonian developed in Ref. [17] is employed. In this effective Hamiltonian, the internal energy is given by $E_{\text{int}}(\{\boldsymbol{u}_i\},\{\boldsymbol{v}_i\},\{\eta_H\},\{\sigma_j\})$. Here $\boldsymbol{u}_i$ is the local (Zr or Ti-centered) soft mode in unit cell i,

which is directly proportional to the local electric dipole moment in that cell. $\{\boldsymbol{v}_i\}$ is the Ba-centered dimensionless local displacements that are related to the inhomogeneous strain variables inside each cell[30,31], while η_H is the homogeneous strain tensor. Finally, $\{\sigma_j\}$ characterizes the atomic configuration of the BZT solid solution, that is σ_j = +1 or -1 corresponds to the presence of a Zr or Ti atom located at the lattice site j, respectively.

The effective Hamiltonian for perovskites approach was first developed in Ref. [31], which contains five energy terms: (i) the local mode self-energy; (ii) the long-range dipole-dipole interaction; (iii) the energy due to short-range interaction; (iv) the elastic energy; and (v) the energy due to the interaction between local mode and strain. While the first two terms are directly related to dipoles, which is important for ferroelectric materials, the last three terms are all related to elastic energy. It is worth noting that the effects of $\boldsymbol{u}_i$ are two-fold: (i) it represents the local mode (see Eq. (5) of Ref. [31]); (ii) it represents the local lattice distortion (since its origin is an optic phonon), and thus giving rise to an elastic energy, namely the short-range interactions, as shown in Eq. (9) of Ref. [31]. In addition to the short-range interaction, the effective Hamiltonian also includes both homogeneous strain (η_H) and inhomogeneous strain ($\boldsymbol{v}_i$). Therefore elastic energies have been properly included in our effective-Hamiltonian-based MC simulations.

In this study, the distribution of the Zr and Ti ions is chosen to mimic the SL structure, which are kept frozen in all the simulations. We use a $12 \times 12 \times 12$ supercell (8640 atoms) to mimic such a system and 160,000 MC sweeps to relax the system at each temperatures. The system is cooled down from 1000 K to 10 K with a step size of 10 K to obtain static properties. In addition, direct *ab initio* calculations are performed to verify the novel phases observed in MC simulations[32].

III. RESULTS AND DISCUSSION

Let us first examine the phases of the BZT SLs at different temperatures. Figure 1(a) shows the supercell-averaged local mode $\langle u_x \rangle$, $\langle u_y \rangle$, $\langle u_z \rangle$ and the average of magnitude, $\langle |\boldsymbol{u}| \rangle$. As we can see, $\langle |\boldsymbol{u}| \rangle$ is always larger than $\langle u_i \rangle$ ($i = x, y, z$), indicating that dipole orientations still have strong randomness even at the lowest temperature. In other words, this system remain macroscopically paraelectric down to the lowest temperatures although $\langle u_x \rangle$ and $\langle u_y \rangle$ have slightly larger magnitudes below $T \simeq 100$ K, indicating a phase transition happens at $T_C \sim 150$ K (note $\langle u_z \rangle$ is zero for all temperatures). To understand the temperature dependency of local modes, Fig. 1(b) shows a snapshot of the dipole configuration of the system at 10 K, which exhibits some interesting

features: (i) Large dipoles only exist on Ti sites, therefore only 6 layers of dipoles can be seen; (ii) All the dipoles stay inside the (001) planes, pointing along one of the four $\langle 110\rangle$ directions; (iii) In a given Ti layer, most of the dipoles have the same y component d_y, but their x component, d_x, can be different and form 90° domains [see Figs. 1(c) and 1(d)]; (iv) Two dipoles from different Ti layers can be parallel, anti-parallel, or perpendicular to each other, indicating the correlation between dipoles in different layers is weaker than that within the same layer. Interestingly, these observations suggest a system that strongly resembles magnetic sheets, where magnetic planes are separated by nonmagnetic materials. For instance, in K_2NiF_4, the antiferromagnetic Ni^{2+} does not couple between adjacent planes[8]. Here in BZT SLs, magnetic dipoles are replaced by electric dipoles. Moreover, it appears that one rule of forming dipole patterns is to avoid head-to-head and tail-to-tail dipole pairs. But exceptions do exist as Figs. 1(c) and 1(e) show the existence of vortices and anti-vortices, which form at the intersections of four nanodomains (shown in different colors) and contain head-to-head or tail-to-tail dipole pairs. Such vortex and anti-vortex structures are known in magnetic systems[33] and $BiFeO_3$[34]. The existence such structures in the BZT SLs further emphasizes the similarity between electric dipole sheets and magnetic dipole sheets.

Clearly, the two observations (iii) and (iv) explain why $\langle u_x\rangle$ and $\langle u_y\rangle$ are minuscule even at the lowest temperature. In addition, similar to the magnetic sheets, where 2D Heisenberg model had shown various interesting phase transitions and patterns of magnetic moments[8,35–38], Fig. 1 shows that the 2D electric dipole system can also have complicated patterns, resembling a frustrated system. The observations (i)–(iv) can be easily explained qualitatively. First, since the lattice constant of BZO is larger than BTO[39], Ti layers effectively experience a tensile strain in the x-y plane and it is hard to develop local mode along z because in this direction the lattice is compressed. Second, it is well known that at low temperature BTO has the $R3m$ phase with local dipoles along $[111]$[30]. Here since polarization along the $[001]$ is disfavored, it is natural that the dipoles point along $\langle 110\rangle$. Third, since Zr has a larger radius, when BTO and BZO are put together (as in the SL), effectively, the BTO layers has a larger lattice constant, and therefore smaller short-range interaction[31], than its natural state, therefore the ions may have more freedom in their movement (i.e., not necessarily along a singe $\langle 110\rangle$ direction). In addition, the dipole-dipole interaction is also weakened since the dipole-dipole interaction is reduced from 3D to 2D. This explains why in the Ti layers, the orientations of dipoles seem to have more freedom. Finally, the dipole-dipole interaction between Ti layers is weak as the distance is doubled compared to that of BTO. In addition, the interaction could be screened due to the existence of Zr layers. This explains why there is essentially no

dipole correlations between Ti layers.

A. Various dipole configurations

The qualitative explanation has obviously invoked arguments that are rather speculative. To quantitatively understand the complex dipole configurations in our MC results, we performed *ab initio* computation using the QUANTUM ESPRESSO software package[40]. Two versions of the exchange-correlation functionals [namely, the local density approximation (LDA)[41] and the generalized gradient approximation (GGA) of Perdew-Burke-Ernzerhof (PBE)[42]] are used along with ultrasoft pseudopotentials[43] implemented in the GBRV package[44], in which the Ba *5s 5p 5d 6s*, Zr *4s 4p 4d 5s*, Ti *3s 3p 4s 3d*, and O *2s 2p* orbitals were treated as valence orbitals. A plane wave basis with kinetic energy cutoff of 1088 eV was used to ensure the convergence in all the calculations. k-point sampling of $8 \times 8 \times 4$ was used for all the 10-atom supercell, $8 \times 8 \times 2$ for the 20-atom supercell, and $2 \times 8 \times 4$ for the 40-atom supercell (see Fig. 2). The initial positions of the atoms are constructed from our MC simulation results, which are then further relaxed until all the force components on each atom are less than 10^{-4} Hatree/Bohr. We note, in all the *ab initio* computations except the $P4mm$ structure [Fig. 2(a)], we also find the shift of Zr ions is much smaller than that of Ti ions, consistent with MC results that the dipoles are essentially zero on Zr cells. All these results indicate that our MC results indeed show the correct dipole configurations.

In our direct *ab initio* computation, we have set up five SLs with different dipole configurations to compare their energies. Figure 2(a) shows a 10-atom cell that has a local dipole along $[001]$, which has the $P4mm$ symmetry. Figure 2(b) is also a 10-atom cell, but having in-plane dipoles along $[110]$ and the $Amm2$ symmetry. Figures 2(c) and 2(d) show more complicated structures with 20-atom supercells, which mimic the dipoles in different Ti layers. In Fig. 2(c), the dipoles in the two Ti layers are perpendicular to each other (space group $Pma2$), while in Fig. 2(d), the two dipoles are antiparallel to each other (space group $Cmcm$). Both of these two situations can be found in Fig. 1(b). Finally, Fig. 2(e) shows a 40-atom supercell, which is a simplified version of the complex dipole patterns observed in a single Ti layer. In this configuration, the first two dipoles along $\hat{x}$ point along $[\bar{1}\bar{1}0]$, while the next two dipoles point along $[\bar{1}10]$, which has the $Pmc2_1$ symmetry[45,46]. In other words, while every layer has the same dipole pattern, in each layer, the dipoles are similarly oriented along $\hat{x}$, but their $\hat{y}$ components alternate every two Ti ions along the $[100]$ direction. It is surprising that, this phase is structurally very different

from that of the $Amm2$ phase (for instance, it has a macroscopic polarization along $[100]$, but $Amm2$ has a polarization along $[110]$). Note this configuration features dipole heads connected to other dipoles' tails. It is found that head-to-head dipole configurations are general not stable in *ab initio* computation of small supercells shown in Fig. 1[47]. We also note that in MC simulations using smaller supercell, which contains 20 or 40 atoms, all dipole configurations shown in Fig. 2 [except Fig. 2(a)] are also observed, but appear in different cooling processes or at different MC steps, indicating that these dipole patterns can dynamically transform from one to another.

In Tab. I we compare the energies of different phases that have been described above. Among all the structures we investigated, the $Amm2$ phase [Fig. 2(b)] has the lowest energy. On the other hand, the $P4mm$ phase [Fig. 2(a)], which has dipoles along the $[001]$ direction has a much higher energy, which is 88.22 (LDA) and 179.79 (PBE) meV / 10 atoms higher than the $Amm2$ phase. It is this high energy that prevents the development of polarization along the out-of-plane polarization in the BZT SLs. Interestingly, the other three dipole configurations (the $Pma2$, $Cmcm$ and $Pmc2_1$ phases) are all extremely close in energy to that of the groundstate $Amm2$ phase and are consistent with Ref. [1]. Similar results provided MC simulations are given in the fourth column of Tab. I, where $Amm2$ is also found to be the ground state. Moreover, given Fig. 2(e) has a low energy, it is reasonable to say, if the periodicity along $[100]$ is larger (i.e., the condensed phonon has a wavevector of $X/3 = (1/6, 0, 0)$, $X/4 = (1/8, 0, 0)$ ... in the Brillouin zone), the energy difference could be even smaller as the portion of the interface energy (interface of two 90° domains) decreases. The closeness in energy of all these different phases to the $Amm2$ shows that metastable states of almost degenerate energy can exist in BZT SLs, which explains why our MC results show complex dipole patterns [i.e., our earlier observations (i)–(iv)] that even include vortices and anti-vortices at 10 K. Therefore maintaining a certain orientation of the polarization, which may be necessary in certain application, in a given BTO layer is difficult at room temperature, although it is shown the energy barrier between different polarization orientations could be high[1], because the various dipole patterns shown in Figs. 1(c)–1(e) and many others that correspond to phonons with small wavevectors can bridge the transformation between different polarization. Further investigation, for instance, on BZT SLs under mechanical strain, may be necessary for the purpose of maintaining a certain polarization in a given layer.

Since elastic energy due to lattice distortion can have a profound effect on polarization[48], we decompose the total energy obtained in MC simulations into its constitutional parts (similar to what is done in a previous work[49]) and find that, for the $Amm2$ phase [Fig. 2(b)] at 5 K, the

short-range interaction[50] is 195.86 meV/10 atoms and comparable in magnitude to that of the dipole-dipole interaction (–370.17 meV/10 atoms). This result indicates that the energy arising from both intra-plane and inter-plane couplings of distorted lattice cells is an important part of the total energy. Table I also shows energies due to the dipole-dipole interaction and the short-range interaction for various dipole configurations. The tiny difference in the short-range interactions between the $Amm2$, $Pma2$, and $Cmcm$ phases, which have very different polarization in adjacent Ti layers, indicates that the elastic couplings between Ti layers are very small. On the other hand, the relatively large values of the $Pmc2_1$ phase indicate that intra-layer interactions are stronger than that of the inter-layer. This situation arises because the small lattice distortion in Zr layers (indicated by the small dipoles associated with Zr sites) make them effective buffer layers to reduce couplings between Ti layers, which is the main cause of independent electric dipole sheets in BZT SLs.

Finally, since epitaxial strain can strongly shape polarization in thin films[48,51,52], we numerically investigated how the epitaxial strain can change dipole configurations in BZT SLs. For instance, at a compressive strain ($\lesssim -4\%$), the $P4mm$ phase has a lower energy than the $Amm2$ phase, thus become energetically favorable. In contrast, the energy difference between the $Pma2$ (or $Cmcm$) phase and the $Amm2$ phase increases quickly with a tensile strain, and become larger than a hundred meV / 10 atoms at $\sim 9\%$, thus the $Pma2$ (or $Cmcm$) phase will likely disappear in the BZT SL in favor of the $Amm2$ phase.

B. Electrostriction

Having investigated the phase structures and dipole configurations of the BZT SLs, we now use MC simulations to check if such a system offers any improved properties over the disordered system. In particular, we examine the polarization and strain variation versus a dc electric field E applied along the $[001]$ direction, which provides information regarding static dielectric and electrostrictive properties [Figs. 3(a)–3(d)]. For (001)-ordered BZT, the polarization P_z is linear with E below $E = 5.2 \times 10^8$ V/m and continues to be linear with E above, but with a smaller slope (i.e., a smaller dielectric constant). Interestingly, Fig. 3(c) shows that the strain versus E curve is perfectly quadratic for $E < 5.2 \times 10^8$ V/m, which implies a strong electrostrictive effect (but no piezoelectric). As a comparison, we also simulated a disordered BZT, which are shown in Figs. 3(b) and 3(d). As we can see, for the dielectric constant, the first linear region is smaller

(below $E = 2.5 \times 10^8$ V/m instead of 5.2×10^8 V/m). The values of the static relative permittivity in the linear region for ordered and disordered systems are 84.7 and 101.6, respectively. More significantly, the electrostrictive strain is much smaller. Figures 3(e) and 3(f) show the variation of homogeneous strain with respect to the polarization for the ordered and disordered systems. To quantify the electrostriction effect, we employ the expression $S_{ij} = Q_{ijkl}P_kP_l$ to fit the curves in Figs. 3(e) and 3(f), where S_{ij} represents strain tensors and Q_{ijkl} are electrostrictive coefficients. It is found that for ordered BZT $Q_{11} = 0.25\,\mathrm{m}^4/\mathrm{C}^2$ and $Q_{12} = 0.10\,\mathrm{m}^4/\mathrm{C}^2$, meanwhile for the disordered BZT $Q_{11} = 0.19\,\mathrm{m}^4/\mathrm{C}^2$ and $Q_{12} = 0.074\,\mathrm{m}^4/\mathrm{C}^2$. The large theoretical values of electrostriction coefficients suggest that BZT is worth further experimental investigation[53]. We also note the range of quadratic electrostriction coefficient in disordered system is much smaller than the ordered BZT SLs.

Moreover, we also obtained the polarization response to the electric field (applied along the $[001]$ direction) at a compressive strain of -5% (where $P4mm$ phase is used since it is the ground state) and a tensile strain of $+9\%$ (where the $Amm2$ phase is used). We found that the the strain is linearly dependent on the polarization P_z, resulting in pizeoelectric effect at a compressive strain of -5%. On the other hand, at the tensile strain of $+9\%$, we find $Q_{11} = 0.2\,\mathrm{m}^4/\mathrm{C}^2$, which is slightly smaller than that of the BZT SLs without any in-plane strain constraint.

IV. SUMMARY

In summary, we have studied the dipole configurations and some basic properties of BZT SLs, and shown that, due to the existence of metastable states, complex dipole configurations and domains of different dipole orientations may exist. It is worth noting that complex dipole patterns are observed in $BaTiO_3$ quantum dots and wires[54], and in compositionally modulated (Ba,Sr)TiO_3 where geometric frustration were observed[55]. Such energy degeneracy and the resulting frustration of dipole configurations are mostly known in magnetic systems, where the Ising model had been employed for theoretical investigation[4–7,10,11], while much less known in electric dipole systems. With our findings here, it can be concluded that, due to energy degeneracy, frustration-like dipole configurations could exist in 0D, 1D, 2D, and 3D electric dipole systems.

In addition, it is rather interesting that such a conventional system[56–58] effectively form 2D electric dipole sheets[1], possessing frustration-like states, and strongly resembling magnetic sheets. We believe this special system deserves more attention: (i) There are many possibilities to grow

SLs with BTO and BZO, for instance, along the $[110]$ and the $[111]$ directions (the Ti layers will have a distance of $2a_{\text{lat}}/\sqrt{2}$ and $2\sqrt{3}a_{\text{lat}}/3$, respectively, where a_{lat} is the distance between a Ti site and its nearest Zr site). It will be interesting to know if such tuning of the distance between Ti ions will affect properties of BZT or induce phenomena that are unknown in disordered BZT. In particular, one may wonder if the relaxor properties can still exist in ordered systems ; (ii) A systematical investigation on the effects of epitaxial strain may reveal other novel phenomena as the misfit strain is tuned. For instance, the $Pmc2_1$ could be the ground state as it happens in $PbTiO_3$ and $BiFeO_3$[45,46]; (iii) Complex dipole configurations (e.g., 2D vortex structures) in the BTO/BZO 2D electric dipole system need to be experimentally investigated. We note, recently the field-induced domain distortion in the $PbTiO_3/SrTiO_3$ SLs had been experimentally demonstrated[28], showing the feasibility of such investigations. Therefore by investigating such a 2D system, we hope it expands our understanding of chemically ordered BZT and will encourage other studies on this interesting system.

Acknowledgments

Discussions with Drs. L. Bellaiche, S. Prosandeev, A. Bokov, J. Petzelt, Z.-G. Gui, and X.-J. Lou are greatly acknowledged. This work is financially supported by the National Natural Science Foundation of China (NSFC) grant 51390472 and NSF grant DMR-1066158. F.L. acknowledges the NSFC grant 51102193. Z.J. acknowledges the support from the 111 Project (B14040). We thank Shanghai Supercomputer Center for providing resources for DFT computations. Some computations were also made possible thanks to the MRI grant 0722625, MRI-R2 grant 0959124, and CI-TRAIN grant 0918970 from NSF.

---

* Electronic address: dawei.wang@mail.xjtu.edu.cn

[1] A. I. Lebedev, Phys. Solid State **55**, 1198 (2013).

[2] E. Manousakis, Rev. Mod. Phys. **63**, 1 (1991).

[3] C. Stamm, F. Marty, A. Vaterlaus, V. Weich, S. Egger, U. Maier, U. Ramsperger, H. Fuhrmann, D. Pescia, Science **282**, 449 (1998).

[4] A. J. Steele, T. Lancaster, S. J. Blundell, P. J. Baker, F. L. Pratt, C. Baines, M. M. Conner, H. I. Southerland, J. L. Manson, and J. A. Schlueter, Phys. Rev. B **84**, 064412 (2011).

[5] I. Morgenstern, K. Binder, and R. M. Hornreich, Phys. Rev. B **23**, 287 (1981).

[6] E. T. Gawlinski, Martin Grant, J. D. Gunton, and K. Kaski, Phys. Rev. B **31**, 281 (1985).

[7] R. Moessner and S. L. Sondhi, Phys. Rev. B **63**, 224401 (2001).

[8] J. M. D. Coey, *Magnetism and magnetic materials*, (Cambridge University Press, New York) 2010.

[9] R. Matzdorf, Z. Fang, Ismail, J. Zhang, T. Kimura, Y. Tokura, K. Terakura, E. W. Plummer, Science **289**, 746 (2000).

[10] J. R. Iglesias, S. Goncalves, O. A. Nagel, and M. Kiwi, Phys. Rev. B **65**, 064447 (2002).

[11] E. A. Jagla, Phys. Rev. E **70**, 046204 (2004).

[12] A. I. Lebedev, Phys. Solid State **53**, 2463 (2011).

[13] T. Maiti, R. Guo, and A. S. Bhalla, J. Am. Ceram. Soc. **91**, 1769 (2008).

[14] V. V. Shvartsman, J. Zhai, and W. Kleemann, Ferroelectrics **379**, 77 (2009).

[15] T. Maiti, R. Guo, and A. S. Bhalla, Ferroelectrics **425**, 4 (2011).

[16] W. Kleemann, S. Miga, J. Dec, and J. Zai, Appl. Phys. Lett. **102**, 232907 (2013).

[17] A. R. Akbarzadeh, S. Prosandeev, E. J. Walter, A. Al-Barakaty, and L. Bellaiche, Phys. Rev. Lett. **108**, 257601 (2012).

[18] S. Prosandeev, D. Wang, A. R. Akbarzadeh, B. Dkhil, and L. Bellaiche, Phys. Rev. Lett. **110**, 207601 (2013).

[19] S. Prosandeev, D. Wang, and L. Bellaiche, Phys. Rev. Lett. **111**, 247602 (2013).

[20] D. Sherrington, Phys. Rev. Lett. **111**, 227601 (2013).

[21] R. Pirc and Z. Kutnjak, Phys. Rev. B **89**, 184110 (2014).

[22] D. Wang, J. Hlinka, A. A. Bokov, Z.-G. Ye, P. Ondrejkovic, J. Petzelt, and L. Bellaiche, Nat. Commun. **5**, 5100 (2014).

[23] F. Li, L. Jin, Z. Xu, and S. Zhang, Appl. Phys. Rev. **1**, 011103 (2014).

[24] A. M. George, J. Iniguez, and L. Bellaiche, Nature **413**, 54 (2001).

[25] C. H. Lee *et al*, Nature **502**, 532 (2013).

[26] S. Lisenkov and L. Bellaiche, Phys. Rev. B **76**, 020102 (2007).

[27] Y. L. Li, S. Y. Hu, D. Tenne, A. Soukiassian, D. G. Schlom, X. X. Xi, K. J. Choi, C. B. Eom, A. Saxena, and T. Lookman, Q. X. Jia, and L. Q. Chen, Appl. Phys. Lett. **91**, 112914 (2007).

[28] P. Chen, M. P. Cosgriff, Q. Zhang, S. J. Callori, B. W. Adams, E. M. Dufresne, M. Dawber, and P. G.

Evans, Phys. Rev. Lett. **110**, 047601 (2013).

[29] I. B. Misirlioglu, M. T. Kesim, and S. P. Alpay, Appl. Phys. Lett. **104**, 022906 (2014).

[30] W. Zhong, D. Vanderbilt, and K. M. Rabe, Phys. Rev. Lett. **73**, 1861 (1994).

[31] W. Zhong, D. Vanderbilt, and K. M. Rabe, Phys. Rev. B **52**, 6301 (1995).

[32] In both MC simulations and in *ab initio* calculations, oxygen octahedra tiltings are not considered as we concentrate on electric dipoles. It is known for BZT SLs, the oxygen octaherda tiltings exist in $BaZrO_3$ layers, not directly to electric dipoles, which mostly exist in $BaTiO_3$ layers[1].

[33] D. H. Lee, J. D. Joannopoulos, J. W. Negele, and D. P. Landau, Phys. Rev. B **33**, 450 (1986).

[34] N. Balke, *et al*, Nat. Phys. **8**, 81 (2012).

[35] P. A. Serena, N. García, and A. Levanyuk, Phys. Rev. B **47**, 5027 (1993).

[36] L. Siurakshina, D. Ihle, and R. Hayn, Phys. Rev. B **64**, 104406 (2001).

[37] H. W. J. Blöte, W. Guo, and H. J. Hilhorst, Phys. Rev. Lett. **88**, 047203 (2002).

[38] D. S. Deng, X. F. Jin, and R. Tao, Phys. Rev. B **65**, 132406 (2002).

[39] The experimental lattice constant of $BaZrO_3$ ($BaTiO_3$) is 4.19 (4.01) Å and therefore the misfit strain is estimated to be $\sim 4\%$ considering the fact that the lattice constant of the SL is between that of $BaTiO_3$ and $BaZrO_3$.

[40] P. Giannozzi, S. Baroni, N. Bonini, M. Calandra, R. Car, C. Cavazzoni, D. Ceresoli, G. L. Chiarotti, M. Cococcioni, I. Dabo, A. D. Corso, S. d. Gironcoli, S. Fabris, G. Fratesi, R. Gebauer, U. Gerstmann, C. Gougoussis, A. Kokalj, M. Lazzeri, L. Martin-Samos, N. Marzari, F. Mauri, R. Mazzarello, S. Paolini, A. Pasquarello, L. Paulatto, C. Sbraccia, S. Scandolo, G. Sclauzero, A. P. Seitsonen, A. Smogunov, P. Umari, and R. M. Wentzcovitch, J. Phys.: Condens. Matter **21**, 395502 (2009).

[41] D. M. Ceperley and B. J. Alder, Phys. Rev. Lett. **45**, 566 (1980); J. P. Perdew and A. Zunger, Phys. Rev. B **23**, 5048 (1981).

[42] J. P. Perdew, K. Burke, and M. Ernzerhof, Phys. Rev. Lett. **77**, 3865 (1996).

[43] D. Vanderbilt, Phys. Rev. B **41**, 7892 (1990).

[44] K. F. Garrity, J. W. Bennett, K. M. Rabe and D. Vanderbilt, Comput. Mater. Sci. **81**, 446 (2014).

[45] Y. Yang, W. Ren, M. Stengel, X. H. Yan, and L. Bellaiche, Phys. Rev. Lett. **109**, 057602 (2012).

[46] Y. Yang, J. Íñiguez, A. J. Mao, and L. Bellaiche, Phys. Rev. Lett. **112**, 057202 (2014).

[47] Head-to-head (or tail-to-tail) dipoles may indeed exist in the $BaTiO_3$/$BaZrO_3$ SLs as seen in Figs. 1(c) and 1(e) along with vortices and anti-vortices. We believe the dipole structure shown in Fig. 1(e) is also a low-energy dipole configuration (i.e., a few meV per ten atoms higher than the ground state). However,

due to their scale (more than1000 atoms will be needed), we are not able to perform direct *ab initio* calculation to find their energy.

[48] N. A. Pertsev, and H. Kohlstedt, Phys. Rev. Lett. **98**, 257603 (2007).

[49] Z. Jiang, R. Zhang, D. Wang, D. Sichuga, C. L. Jia, and L. Bellaiche, Phys. Rev. B **89**, 214113 (2014).

[50] The short-range interaction arises due to displacements of ions in neighboring lattice cells[31]. This type of lattice distortion is directly related to the electric dipole in each unit cell. For the BZT SL studied here, we find the elastic energy directly related to homogeneous and inhomogeneous strain is much smaller than that due to the short-range interaction (the former is only about 5% of the latter). In addition, the $Amm2$, $Pma2$, $Cmcm$ and $Pmc2_1$ phases have essentially the same elastic energy that is directly related to homogeneous and inhomogeneous strain (the relative difference is no more than 4%). These two facts indicate that lattice deformation (strain) is a less important factor to consider than ion displacements associated with electric dipoles.

[51] N. A. Pertsev, A. G. Zembilgotov, and A. K. Tagantsev, Phys. Rev. Lett. **80**, 1988 (1998).

[52] N. A. Pertsev, V. G. Kukhar, H. Kohlstedt, and R. Waser, Phys. Rev. B **67**, 054107 (2003).

[53] The experimental value of Q_{11} = 0.11 m^4/C^2 for $BaTiO_3$, and 0.02–0.06 for disordered PMN-PT[23].

[54] H. Fu, and L. Bellaiche, Phys. Rev. Lett. **91**, 257601 (2003).

[55] N. Choudhury, L. Walizer, S. Lisenkov and L. Bellaiche, Nature **470**, 513 (2011).

[56] T. Tsurumi, T. Ichikawa, T. Harigai, H. Kakemoto, and S. Wada, J. Appl. Phys. **91**, 2284 (2002).

[57] P. R. Choudhury and S. B. Krupanidhi, Appl. Phys. Lett. **92**, 102903 (2008).

[58] M. E. Marssi, Y. Gagou, J. Belhadi, F. D. Guerville, Y. I. Yuzyuk, and I. P. Raevski, J. Appl. Phys. **108**, 084104 (2010).

Figure 1: (Color online) The average Cartesian components and absolute magnitude of the local mode vectors as a function of temperature are shown in Panel (a). The inset of Panel (a) displays the unit cell of the BZT SLs. A snapshot of dipole configuration of the BZT SLs at 10 K is shown in Panel (b). The dipole structures from the first, second, and fourth layer (counting from bottom along z and only layers containing Ti ions are counted) are shown in Panels (c)–(e). Four different colors are used to denote dipoles of different orientations (one of the four $\langle 110 \rangle$ directions).

Figure 2: (Color online) Five dipole configurations are shown and their total energies are calculated using density functional theory (see text). In Panels (a)–(e), the directions of dipoles on each Ti site are shown as blue arrows (also see Tab. I). Four of these configurations in Panels (b)–(e), which are suggested by MC simulations, are found to be low-energy states.

Space group	ΔE (LDA) [a]	ΔE (PBE)	ΔE (MC)[b]	Dipole-dipole (MC)	Short-range (MC)	Dipole
$P4mm$ (#99)	88.22	179.79	–	–	–	$[001]$
$Amm2$ (#38)	0.00	0.00	0.00	0.00	0.00	$[110]$
$Pma2$ (#28)	2.48	3.93	0.17	-0.03	0.63	$[110]\&[\bar{1}10]$
$Cmcm$ (#63)	2.93	3.58	0.05	-0.75	1.52	$[110]\&[\bar{1}\bar{1}0]$
$Pmc2_1$ (#26)	2.05	2.96	1.37	-19.01	22.56	$[\bar{1}\bar{1}0]\&[\bar{1}10]$

[a]The energy unit is meV per 10 atoms.

[b]MC simulations are performed at $T = 5$ K

Table I: The energies of various dipole configurations of the BZT SLs. The $Amm2$ phase is found to be the ground state, which is used as the reference energy. The total energies obtained in MC simulations are decomposed to obtain the energies due to the dipole-dipole interaction and the short-range interaction[31].

Figure 3: (Color online) Polarization (top panel) and strain (middle panel) as a function of an electric field, strain as a function of polarization (bottom panel) for the ordered (left column) and disordered BZT (right column) at 10 K. The electric field is applied along the $[001]$ direction. We note the strain is calculated with reference to the lattice constant $a_0 = 4.047$ Å, which is a starting parameter in MC simulations.

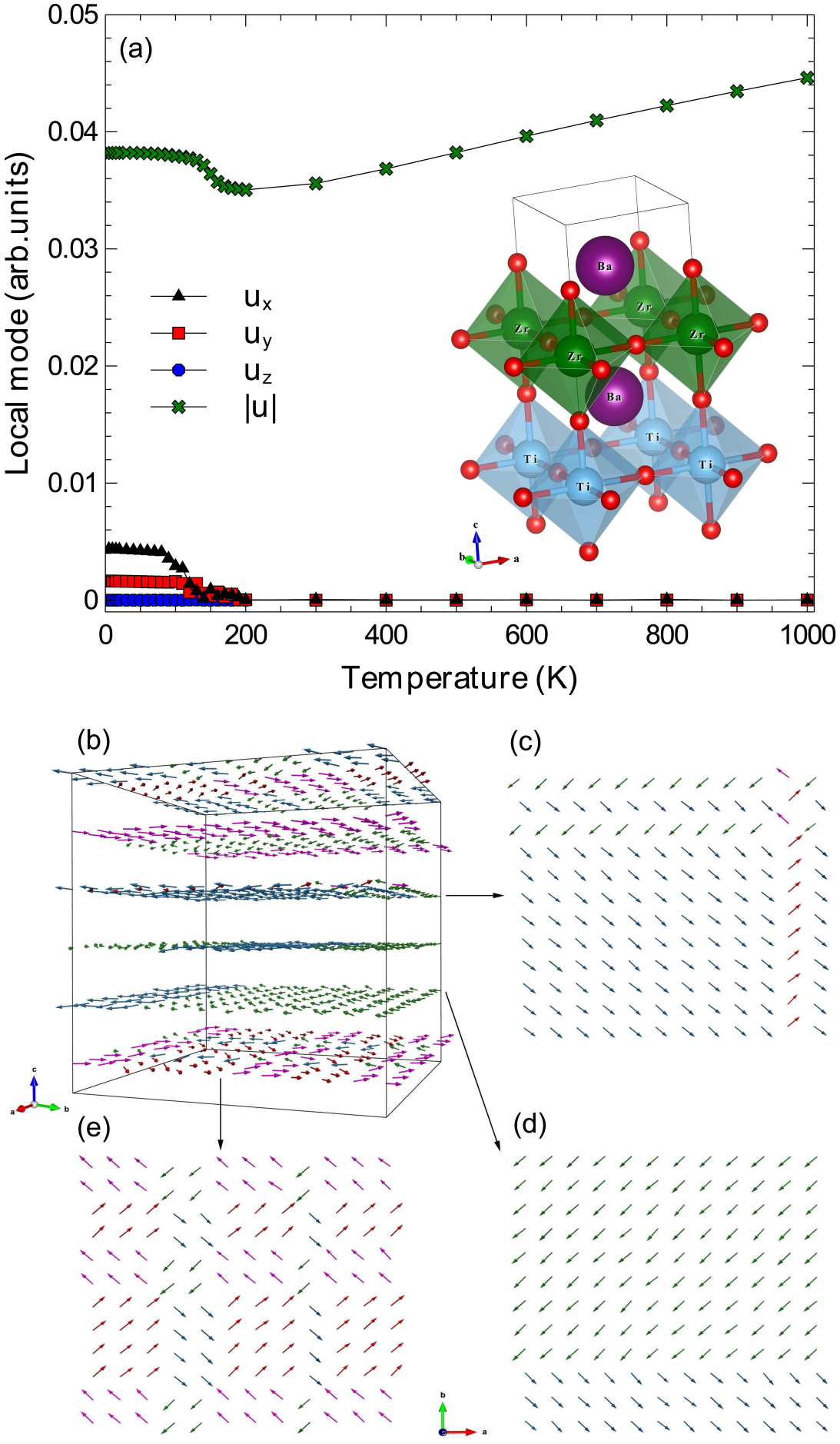

Figure 1 12Nov2014

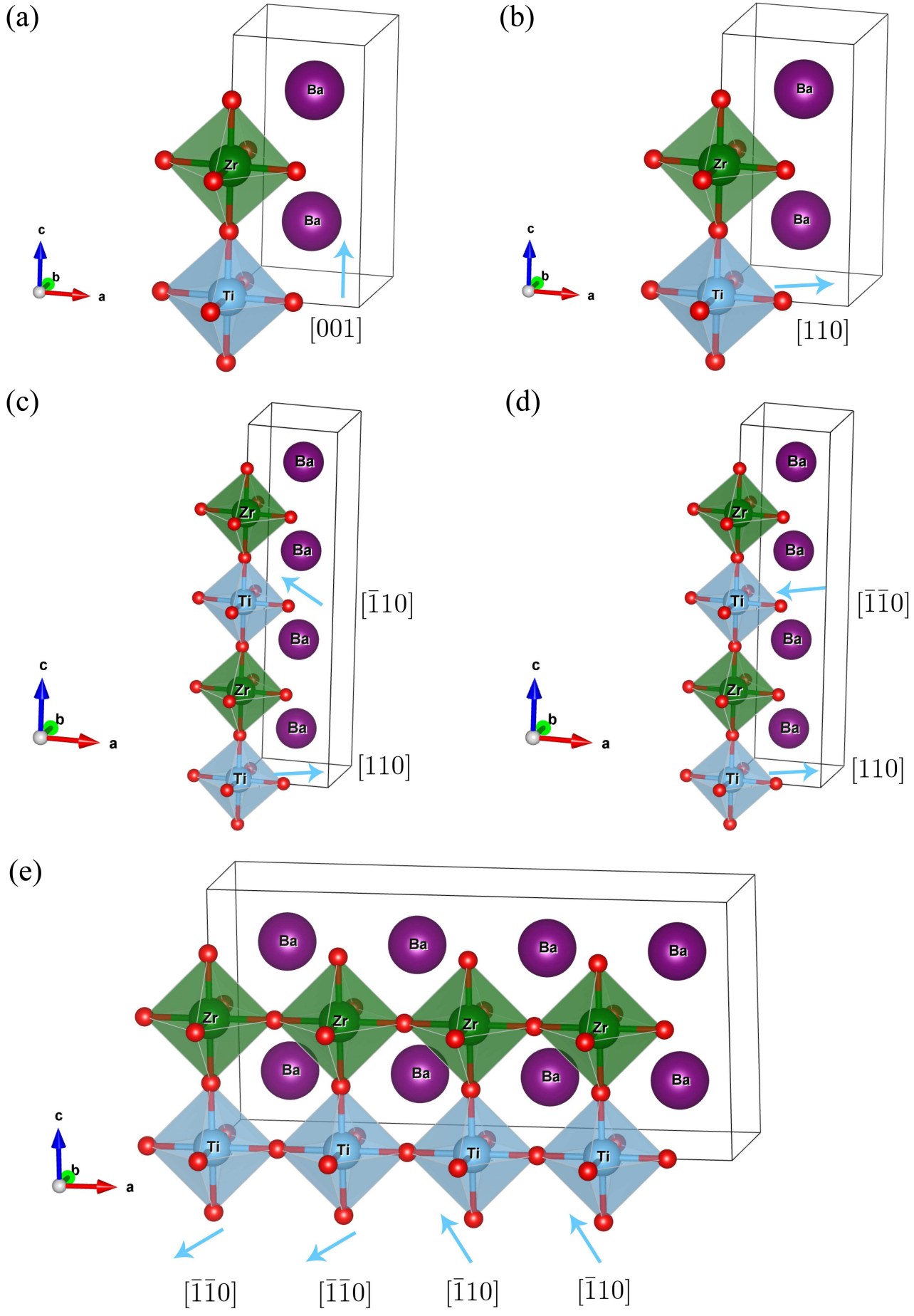

Figure 2 12Nov2014

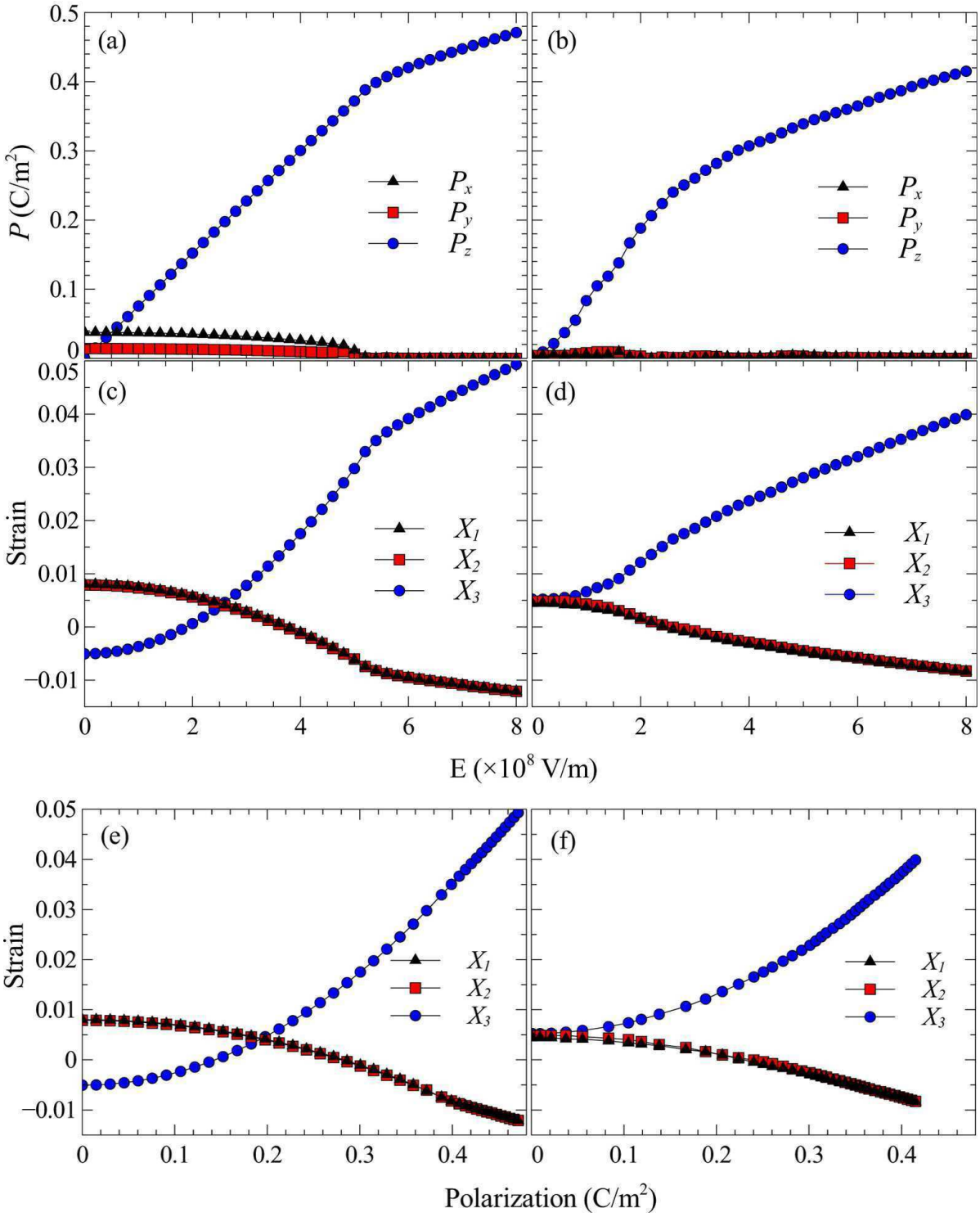

Figure 3 12Nov2014